Int J Adv Manuf Technol (2015) 81:811–823
DOI 10.1007/s00170-015-7251-7

ORIGINAL ARTICLE

A comparison of solid model and three-orthogonal dexelfield methods for cutter-workpiece engagement calculations in three- and five-axis virtual milling

Y. Boz[1] · **H. Erdim**[2] · **I. Lazoglu**[1]

Received: 30 October 2014 / Accepted: 30 April 2015 / Published online: 14 May 2015

Abstract Virtual simulation of three- and five-axis milling processes has started to become more important in recent years in various industries such as aerospace, die-mold, and biomedical industries in order to improve productivity. In order to obtain desired surface quality and productivity, process parameters such as feedrate, spindle speed, and axial and radial depths of cut have to be selected appropriately by using an accurate process model of milling. Accurate process modeling requires instantaneous calculation of cutter-workpiece engagement (CWE) geometry. Cutter-workpiece engagement basically maps the cutting flute entry/exit locations as a function of height, and it is one of the most important requirements for prediction of cutting forces. The CWE calculation is a challenging and hard problem when the geometry of the workpiece is changing arbitrarily in the case of five-axis milling. In this study, two different methods of obtaining CWE maps for three- and five-axis flat and ball-end milling are developed. The first method is a discrete model which uses three-orthogonal dexelfield, and the second method is a solid modeler-based model using Parasolid boundary representation kernel. Both CWE calculation methods are compared in terms of speed, accuracy, and performance for three- and five-axis milling of ball-end and flat-end mill tools. It is shown that the solid modeling-based method is faster and more accurate. The proposed methods are experimentally and computationally verified in simulating milling of complex three-axis and five-axis examples as well as predicting cutting forces.

Keywords Solid modeling · Machining · Milling · Simulation · Free form · Sculptured surface · Cutter-workpiece engagement · Engagement domain · Contact region · Ball-end mill · Flat-end mill · CNC · Boundary representation · 3-Dexelfield

✉ I. Lazoglu
ilazoglu@ku.edu.tr

[1] Manufacturing and Automation Research Center, Department of Mechanical Engineering, Koc University, Sariyer 34450, Istanbul, Turkey

[2] Product Development, The Boeing Company, P.O. Box 3707, Seattle, WA 98124, USA

1 Introduction

The ultimate focus of the manufacturing is to produce parts correctly and most economically on the production floor. The main aims of using virtual machining are stated to reduce cycle times; dimensional and surface errors before the parts are machined on the machine tools [1]. However, this cannot be achieved satisfactorily without the geometrical and physical modeling of the machining processes. Furthermore, while machining free-form surfaces, local peak forces may occur due to spatially changing engagement between the cutter and the workpiece. Hence, cutting force modeling gains more importance in order to prevent excessive cutter deflection and surface errors in these processes.

In free-form surface machining, the cutter-workpiece engagement region does vary along the cutter path, and in general, unless some specific and very simple workpiece geometry is machined, it is difficult to find an exact analytical representation for the engagement region. Chip load and force calculations are based on the cutter/workpiece engagements; therefore, the output of the engagement model is very critical.

The basic idea in numerical control (NC) verification and simulation is to remove the cutter swept volume from the workpiece stock and thus to obtain the final machined surfaces. Mathematically, the swept volume is the set of all points

in space encompassed within the object envelope during its motion. During this verification process, if the contact surface between the tool swept volume and workpiece is calculated at each toolpath segment, cutter-workpiece engagement information is obtained by a further discretization of this contact surface.

In the literature, most of the research has been devoted to discrete simulation of NC machining processes [2–5]. Commonly, these methods use the Z-buffering technique which is primarily used for rendering in computer graphics. Chappel [2] presented a method of using vectors to simulate the material removed by NC milling and developed a method for calculating vector intersections with a cylinder representing a milling cutter.

Drysdale and Jerard [4] developed an approach for simulation of three-axis NC machining of sculptured surfaces. In this method, blank workpiece is represented as a series of Z-vectors on an *X*-*Y* grid. Material removal is simulated by reducing the length of the Z-vector if an intersection occurs with the tool while it is moving. Van Hook [3] used an extended Z-buffer for NC machining simulation where three-axis milling with undercuts (i.e., T-slot machining) and five-axis milling can be simulated. Fussell et al. utilized extended Z-buffer scheme for cutter-workpiece engagement (CWE) calculation in three-axis machining [6] and five-axis machining [7]. In five-axis machining simulation, tool movement is simplified to three-axis moves where each movement is subdivided into smaller segments. Roth et al. developed an adaptive and local depth buffer to calculate cutter-workpiece engagements for three-axis and five-axis machining [8]. This approach aligned the depth buffer to the tool axis orientation and sized the depth buffer to the tool rather than the workpiece. Use of the adaptive and local depth buffer offers less memory storage, less computational load, and increased simulation accuracy.

Solid modeler-based CWE calculation methods may overcome the limitations introduced by discrete methods since the cutter and the workpiece can be modeled using geometric primitives or complex geometric shapes. With this knowledge, Voelcker and Hunt [9] were the first researchers to investigate the NC verification from the solid modeling aspect applying Boolean subtraction operation for material removal simulation from the stock workpiece.

Spence and Altintas [10] used a solid modeler-based CWE extraction system for 2.5-axis end milling employing the constructive solid geometry (CSG) representation. Along the toolpath, for each toolpath segment, cutting tool is intersected with all geometric primitives defining the workpiece. Then, cutter-workpiece intersection information for each primitive is combined in order to form the complete engagement region. Updated workpiece (CSG tree) is also stored for further cutting passes. Spence et al. [11] extended solid modeler-based CWE system for the simulation of ball-end milling and five-axis milling by adopting the boundary representation (B-rep) modeler of the ACIS solid modeling kernel.

Imani et al. [12] developed a geometric simulation module for simulating two-axis and three-axis ball-end milling operations using ACIS solid modeling kernel which can extract the chip geometry. Then, Imani et al. [13] enhanced their geometric simulation module [12] for three-axis ball-end milling of free-form surfaces for semi-finishing and finishing operations. Material removal is simulated by subtracting the B-rep model of the tool swept volume from the in-process workpiece, in order to extract the feed-mark and scallop geometries.

More recently, Ferry and Yip-Hoi [14] proposed a semi-discrete solid modeling-based method in order to obtain cutter-workpiece engagement data for five-axis flank milling with tapered ball-end mill tools. In this work, using the ACIS solid modeling kernel tool swept volume is subtracted from the workpiece at each toolpath segment and removal volume is obtained. Then, the removal volume is sliced into a number of parallel planes along the intermediate axis of the two consecutive cutter locations, and the intersection curves are determined. Finally, endpoints of the intersection curves are joined with lines for forming the engagement polygon where the engagement domain is calculated from this polygon.

This paper investigates two different computational approaches for the extraction of the cutter-workpiece engagement in NC machining, namely solid modeler-based (SM) and three-orthogonal dexelfield (3-OD). In the context of this study, accuracy, speed, and the performance of these methods are compared on different kinds of machining strategies such as three- and five-axis machining. The paper is organized as follows. Section 2 summarizes the basics of the geometrical relations in the cutter-workpiece engagement calculation which is common in both approaches. SM and the 3-OD schemes are described in Section 3 and 4, respectively. In Section 5, we discuss the associated prototype implementation of these two methods together with several different examples, and in the following subsections, we present a detailed comparison of these two methods with related computational issues and practical applications in predicting cutting forces as well. Finally, Section 6 concludes the paper by drawing attention to the main findings and the importance of this work.

2 Cutter-workpiece engagement model

The process methodology presented in this study is given in Fig. 1. The current paper focuses on cutter-workpiece engagement extraction which is one of the most important steps in this flowchart. In industry, there are two main machining strategies for five-axis NC machine tools. The first strategy is called point milling where only the tooltip is in contact with the workpiece. It involves taking more light and shallow cuts with a ball-end or tapered ball-end mill tools. However, the

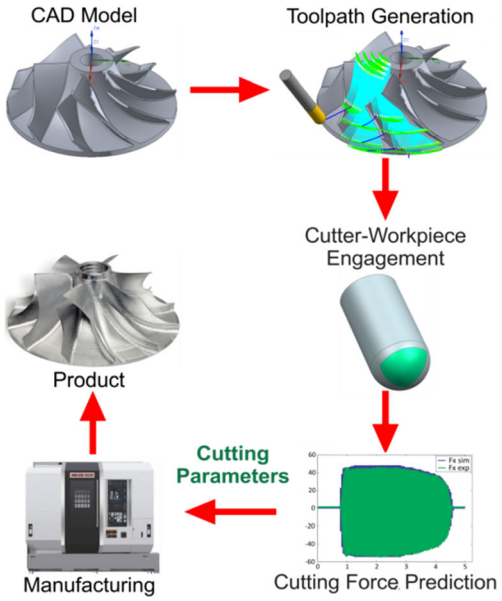

Fig. 1 Process methodology of virtual milling

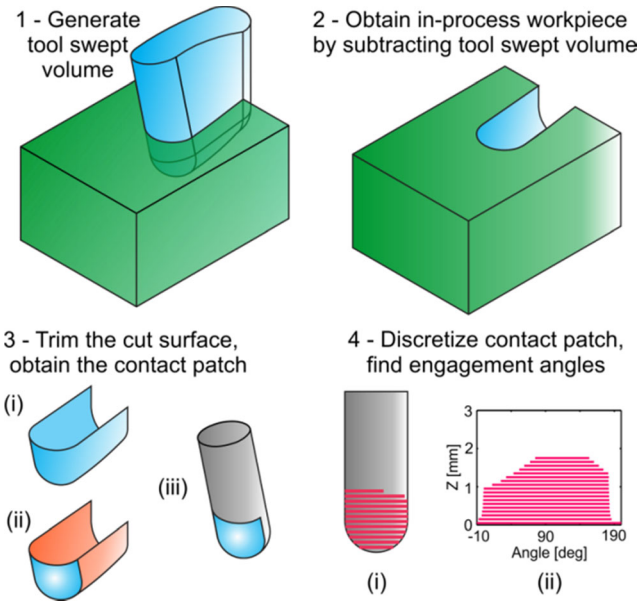

Fig. 2 Engagement extraction flow chart

second strategy, flank milling is a less common machining process. Not only the tooltip but also the side of the cutter is in contact with the workpiece; it is an aggressive form of cutting. Therefore, the tool life is generally shorter and requires much stiffer and more powerful machine tools. Point milling method focuses on the efficiency of material removal rate, machining time, avoidance of global interference and local gouging, surface finish, and scallop heights. Compared to point milling, flank milling is a much less common approach. Therefore, cutter-workpiece engagement calculations for five-axis machining are focused on point milling strategy in this paper. On the other hand, flank milling strategy is an ongoing effort by the authors.

In this study, both solid-based (direct Boolean) method and spatial partitioning method (depth buffer) is utilized. Solid modeler-based (SM) cutter-workpiece engagement method presented in Section 3, and depth buffer method (3-OD) is presented in Section 4. There are several steps performed to obtain cutter-workpiece engagement maps for multi-axis milling as seen in Fig. 2. The first step is the generation of the tool swept volume in order to obtain the in-process workpiece and the contact patch between the tool and the workpiece. In-process workpiece is obtained by subtracting the tool swept volume between consecutive cutter locations from the stock workpiece as shown in Fig. 2, step 2. If the tool swept volume intersects with the workpiece (material removal occurs), there will occur a contact patch between two sets. According to sweep theory [15], engagement domain lies in the egress region of the tool swept envelope. In other words, this can be simplified as the front side of the tool with respect to total move vector. Hence, the contact patch between the tool and the workpiece is obtained by trimming surfaces outside the egress region from the cut surface (Fig. 2, step 3).

Finally, the contact patch is divided into discrete disks along the tool axis and boundary points of these disks are converted into engagement angles with respect to the feeding direction. Some of the steps are explained in further detail in the following sections. The examples are shown for five-axis milling case; however, both approaches can handle easier milling types such as 2.5-axis and three-axis milling cases compared to five-axis tool motions.

2.1 Geometry of multi-axis milling

In three-axis milling, tool movement is given as three translational motions along the *X*-*Y*-*Z* coordinate frame axes. The tool axis is constant during the motion; however, five-axis milling geometry differs from three-axis milling geometry. In five-axis milling, two additional rotary axes are present. Consequently, tool motion is defined as a combination of three translational motions and two rotational motions. Rotational motion in five-axis milling is represented by lead and tilt angles. Lead angle is defined as the rotation angle about $\mathbf{Y}_w$ which is the *Y*-axis of workpiece coordinate frame. The tilt angle is the rotation angle about $\mathbf{X}_w$ which is the *X*-axis of the workpiece coordinate frame. Definition of the lead and tilt angles and the illustration of the coordinate frames are shown in Fig. 3, where ($\mathbf{X}_f$–$\mathbf{Y}_f$–$\mathbf{Z}_f$) is the feed coordinate frame.

2.2 Generation of swept volume and in-process workpiece

One of the first steps in CWE calculation is to generate the solid volume removed by the tool during the cutting process. Schematic illustration of a ball-end mill sweep along three-axis motion is shown in Fig. 4.

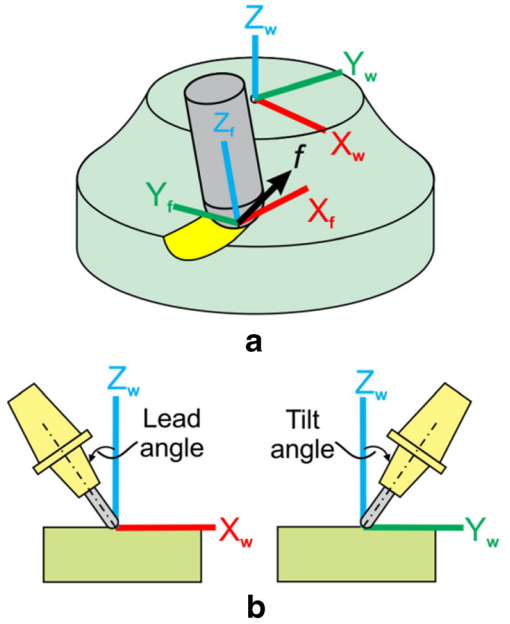

Fig. 3 **a** Illustration of coordinate frames. **b** Lead and tilt angles

As shown in Fig. 4, tool swept volume of a ball-end cutter comprises three regions which are regions of egress points, ingress points, and grazing points. While obtaining the swept volume, the most important parameter is cutting direction since it determines the grazing points together with the geometric properties of the cutter. Simply, egress points represent the front side, ingress points represent the back side, and grazing points represents the swept envelope of the cutter with respect to the cutting direction. Hence, the possible engagement domain of the cutter lies in the egress point region, meaning that the front side of the tool swept volume.

Since we are only dealing with point milling strategy, only the tip of ball-end mill tool will be in contact with the workpiece. Therefore, the swept volume will be computed only for the spherical part of the ball-end mill. Because of the rotational invariance of the sphere, the tip of the ball-end mill, sphere will follow a three-axis motion and form a swept volume similar to three-axis motions. However, transformation needs to be applied to get the right engagement angles as discussed in Section 2.3. According to solid sweep theory [15, 16], three regions shown in Fig. 4 can be obtained as follows:

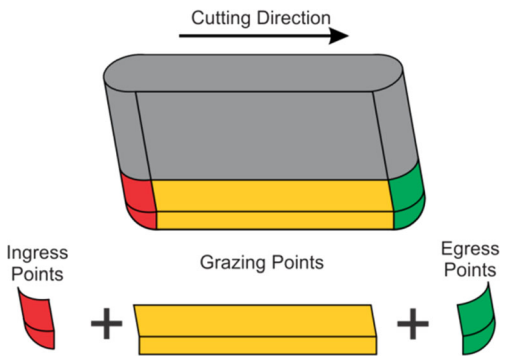

Fig. 4 Tool swept volume of a ball-end mill

$$\begin{array}{ll} \vec{n}\cdot\vec{m}>0 & \text{Egress points} \\ \vec{n}\cdot\vec{m}=0 & \text{Grazing Curve(points)} \\ \vec{n}\cdot\vec{m}<0 & \text{Ingress points} \end{array} \quad (1)$$

where $\vec{n}$ is the surface normal at an arbitrary point on the cutter surface and $\vec{m}$ is the movement vector. Tool motion in five-axis machining also includes an arbitrary rotation, and this effect will be taken into account if swept volume of the cylinder part of the cutter is in a cut in the case of flank milling strategy.

2.3 Calculation of engagement domain from contact patch

Once the contact region between the tool swept envelope and workpiece is obtained, they are transformed (translated) from the workpiece coordinate frame to the tooltip of the cutter as shown in Fig. 5. $\vec{P}_i$ represents the coordinates of the *i*th cutter location (CL) point in the toolpath in the workpiece coordinate frame. The contact patch is the surface obtained by combining all of the intersection points and is transformed into tooltip origin as,

$$\overrightarrow{CV} = \overrightarrow{CP} - \vec{P}_1 \quad (2)$$

where $\overrightarrow{CV}$ is the cut vector in the tooltip origin and $\overrightarrow{CP}$ is the cut point in workpiece coordinate frame. After the transformation given in Eq. (6) is applied, basis of the tool movement vector, feed vector, and feed coordinate frame is defined. Consider two consecutive five-axis tool movements shown in Fig. 6, where tool is first moving from $(i-1)$th CL point to the *i*th CL point and then to the (i+1)th CL point.

For determining the engagement domain for the *i*th CL point, tool swept volume from the $(i-1)$th CL point to the *i*th CL point has to be calculated. Therefore, tool movement vector is defined as,

$$\vec{m} = \left(\vec{P}_i - \vec{P}_{i-1}\right)/\|\vec{P}_i - \vec{P}_{i-1}\| \quad (3)$$

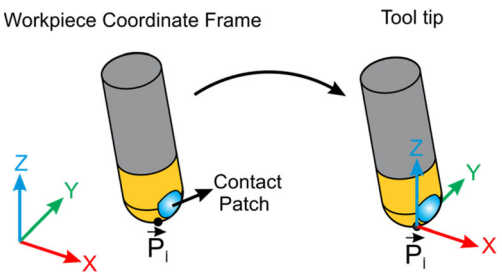

Fig. 5 Transformation from workpiece coordinate frame to the tooltip

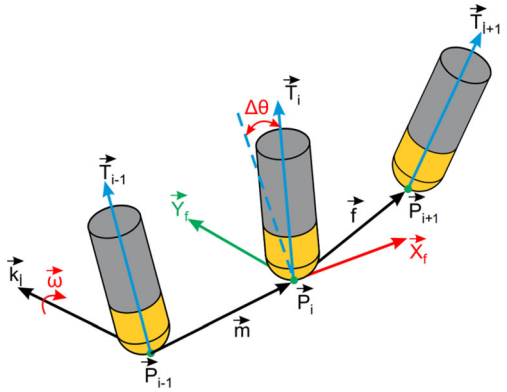

Fig. 6 Basis of the tool movement vector, feed vector, and feed coordinate frame

In five-axis machining, tool can rotate along the axes as well as translate along the tool path. Therefore, during translation tool axis rotates from $\vec{T}_{i-1}$ to $\vec{T}_i$ around an arbitrary axis $\vec{k}_i$, an amount of $\Delta\theta$ where rotation axis is both orthogonal to $\vec{T}_{i-1}$ and $\vec{T}_i$. Rotation axis $\vec{k}_i$ and rotation angle $\Delta\theta$ are calculated as,

$$\vec{k}_i = \frac{\vec{T}_{i-1} \times \vec{T}_i}{\|\vec{T}_{i-1} \times \vec{T}_i\|}$$
$$\Delta\theta = \text{atan2}\left(\frac{\|\vec{T}_{i-1} \times \vec{T}_i\|}{\vec{T}_{i-1} \cdot \vec{T}_i}\right) \quad (4)$$

where atan2 is four quadrant $[-\pi, \pi]$ arctangent function.

Cutting force model use the engagement domain for the ith CL point while cutting tool is moving from the ith CL point to $(i+1)$ the CL point, assuming that in this toolpath segment, cutting forces are the same until tool arrives at $(i+1)$th CL point. In this respect, feed coordinate frame is constructed by using these CL points. Feed vector $\vec{f}$ can be expressed as,

$$\vec{f} = \left(\vec{P}_{i+1} - \vec{P}_i\right) / \|\vec{P}_{i+1} - \vec{P}_i\| \quad (5)$$

Another important property regarding feed coordinate frame is that the feed direction and the cross-feed direction denoted as $\vec{X}_f$ and $\vec{Y}_f$, respectively, have to lie in a plane where the normal of this plane is $\vec{T}_i$. In other words, an orthogonal basis is defined using tool axis vector $\vec{T}_i$ and feed vector $\vec{f}$,

$$\vec{Y}_f = \vec{T}_i \times \vec{f}$$
$$\vec{X}_f = \vec{Y}_f \times \vec{T}_i \quad (6)$$

Here, it is necessary to remind that Z-axis of the feed coordinate frame $\vec{Z}_f$ is coincident with the tool axis orientation $\vec{T}_i$ at cutter location i.

2.4 Determination of engagement quadrants

Start and exit angles of the engagement domain can be identified correctly by checking the quadrant of the engagement angle. The method for the quadrant determination can be given as follows,

$$\begin{aligned} &CV_x > 0, \quad CV_y > 0 \Rightarrow \text{Quadrant I} \\ &CV_x > 0, \quad CV_y < 0 \Rightarrow \text{Quadrant II} \\ &CV_x < 0, \quad CV_y < 0 \Rightarrow \text{Quadrant III} \\ &CV_x < 0, \quad CV_y > 0 \Rightarrow \text{Quadrant IV} \end{aligned} \quad (7)$$

In three-axis machining, engagement region is determined only by the tool movement direction since the tool axis direction is fixed in vertical or horizontal direction. In contrary, tool orientation for five-axis tool motion changes spatially; therefore, possible engagement region is related to moving direction and tool axis orientation. If $\vec{T}_i \cdot \vec{m} > 0$, quadrant I and quadrant II are valid (cutting tool is leading forward, only forward side of the cutter can be in engagement). If $\vec{T}_i \cdot \vec{m} < 0$, quadrant I, quadrant II, quadrant III, and quadrant IV are valid (cutting tool is leading backward, forward, and aft side of the cutter can be in engagement). The method explained above is illustrated in Fig. 7. Then, the engagement angle θ_e is determined as,

$$\theta_e = \text{atan2}\left(CV_x, CV_y\right) \quad (8)$$

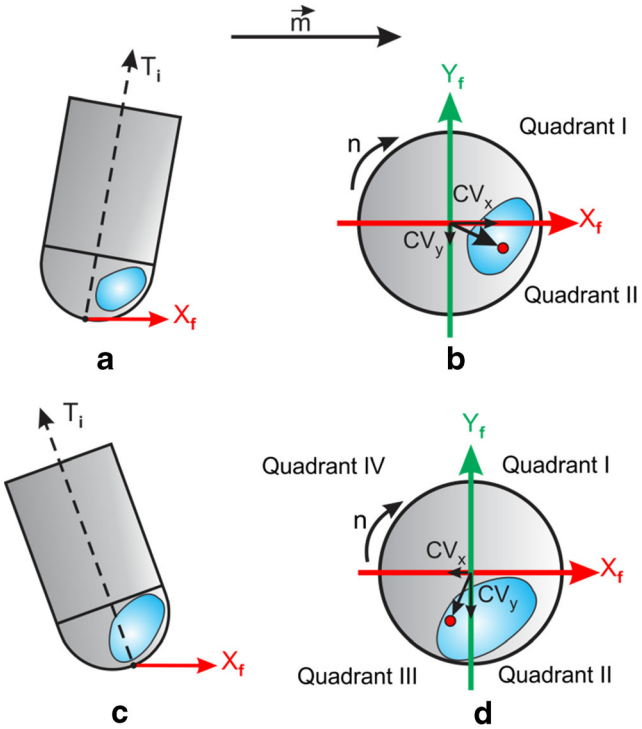

Fig. 7 Engagement quadrant determination: **a** tool move for $\vec{T}_i \cdot \vec{m} > 0$, **b** valid engagement regions for $\vec{T}_i \cdot \vec{m} > 0$, **c** tool move for $\vec{T}_i \cdot \vec{m} < 0$, and **d** valid engagement regions for $\vec{T}_i \cdot \vec{m} < 0$

3 Solid modeler-based engagement domain computation

Currently, the most popular schemes used in solid modelers are the boundary representation (B-rep) and constructive solid geometry (CSG). In the B-rep methodology, an object is represented by both its boundaries defined by faces, edges, vertices, and the connectivity information. The prototype program is implemented using the commercial Parasolid solid modeler kernel. Tool swept volume is obtained by generating the grazing curves of the tool with respect to 3D tool movement vector and sweeping these curves. Egress and ingress volumes are added afterward by Boolean operations. Tool movement vector is defined by two curves from the tool tip and maximum tool height from the starting point to end point. Tool swept volumes are subtracted from the workpiece model by using Boolean functions in order to find the in-process machined surface. Once the in-process workpiece is obtained for each CL point, the contact patch surface between the tool and workpiece is extracted. Then, the resulting 3D contact surface, as illustrated in Fig. 8, is projected to the plane perpendicular to the cutter axis. This step finds the enclosing boundaries and the curves of the contact patch. Since the force model discretizes the cutter into slices perpendicular to the tool axis and to perform force calculation for each slice, the disks at each level are projected to the plane perpendicular to the cutter axis.

Since engagement domain is simply the combination of start and exit angles of each discrete disk located on the cutter, the next step is to assign the start and exit angles to each respective projected disk by intersecting the 2D disks with the boundaries of the contact patch in the plane.

A final step is required to convert the intersection points into start and exit angles that are required for the force prediction model. Cutter-workpiece engagement geometry extraction for ball-end mill is shown in Fig. 8. The procedure described above is implemented in Visual Studio.NET using the Parasolid solid modeling kernel and Parasolid Workshop on a Windows Core2Duo, 1.8 GHz/4 GB personal laptop. The output of the program for engagement angles is shown together with the contact patch for different CL points in Figs. 9 and 10 for impeller workpiece.

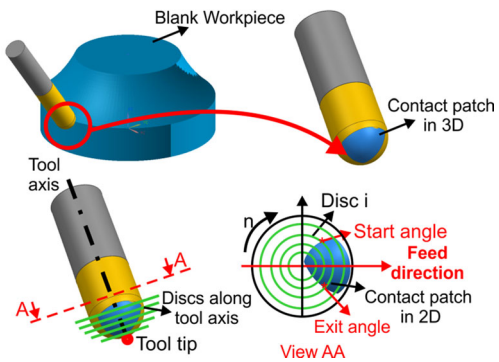

Fig. 8 Cutter-workpiece engagement geometry extraction for ball-end mill

For the first CL point, the engagement domain is one piece (continuous over per tool revolution, one start and exit angle). However, the engagement domain can have more than one piece because of the complexity of the geometry of the workpiece and the tool motion as shown simply in Fig. 11. In this case, the engagement domain will have more than two intersections for the disks along the cutter as seen for CL point #86 shown in Fig. 10. The resulting 3D contact surface for this CL point is illustrated in Fig. 10c and rotated cutting tool in Fig. 10d.

4 Three-orthogonal dexelfield-based engagement domain computation

The most popular and commonly used depth buffer scheme in the literature and in the CAM packages is the Z-buffer method. The Z-buffer method is usually referred as Z-map method. In conventional Z-map method [17], the workpiece is represented as the intersection points of the Z direction vectors (ZDV) with the workpiece surface on a 2D grid of ZDVs. These intersection points are also utmost part of the workpiece

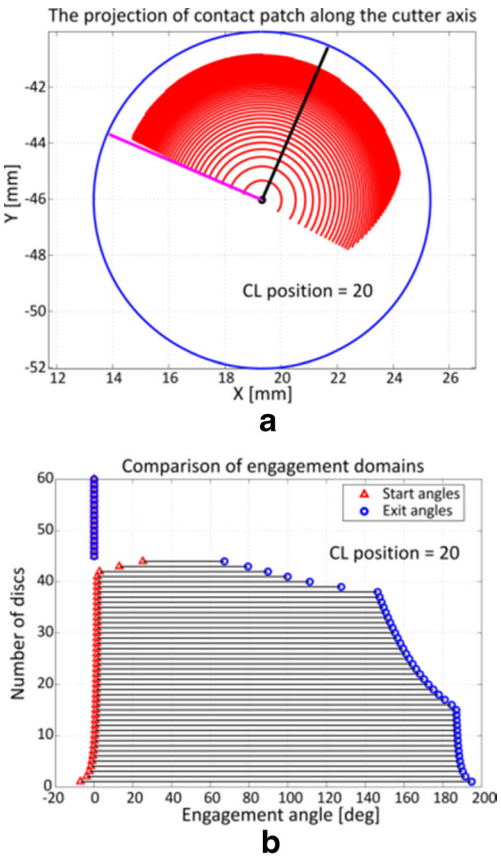

Fig. 9 The engagement domain for CL point #20: **a** projected view of the contact patch along the cutter axis and **b** start and exit angles for the disks along the cutter axis

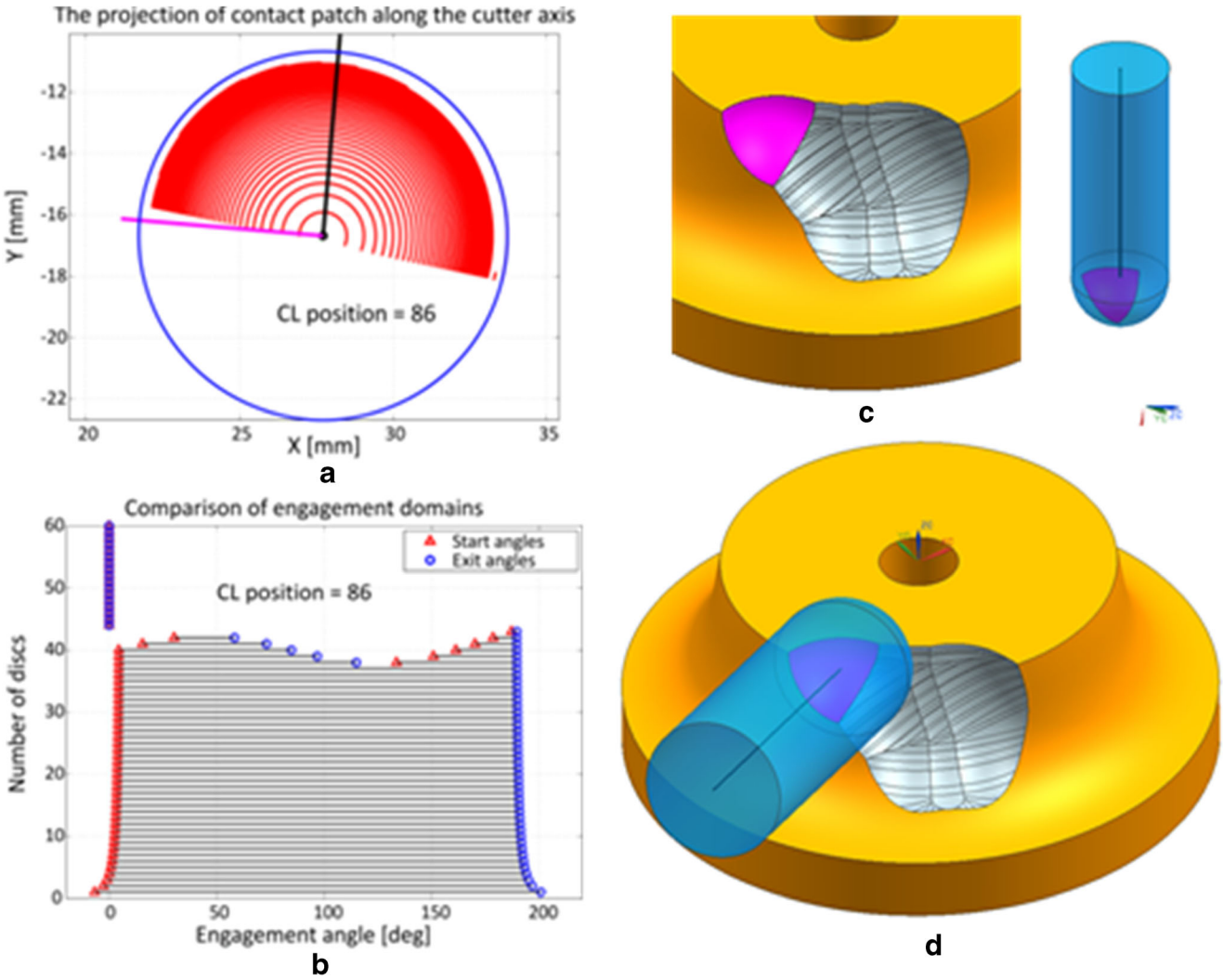

Fig. 10 The engagement domain for CL point #86: **a** projected view of contact patch along cutter axis, **b** start and exit angles for the disks along the cutter axis, **c** contact surface, and **d** contact surface with the five-axis tool motion

surface where only one intersection of the workpiece with a ZDV is permitted.

In five-axis machining, conventional representation is not sufficient because almost all of the parts have walls with negative inclination angle and undercut machining is required. Hence, for five-axis machining, NC simulation extended Z-map approach [7] is utilized. In extended Z-map approach, for one ZDV, multiple intersections and gap elements between the intersection points can also be stored most of the time using a linked list data structure. Conventional and extended Z-map approaches are shown schematically in Fig. 12.

In this paper, a commercial NC verification kernel is used for machining simulation in order to obtain the contact patch between the tool and the workpiece. This verification kernel provides the use of three-orthogonal dexelfield which is

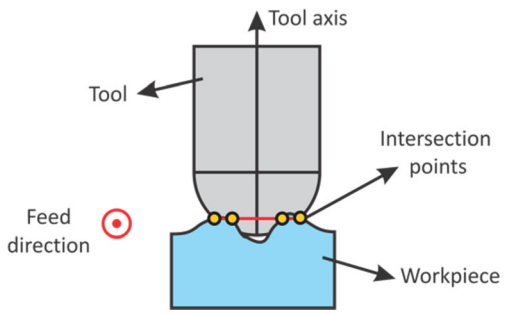

Fig. 11 Illustration of multiple contact regions and intersections

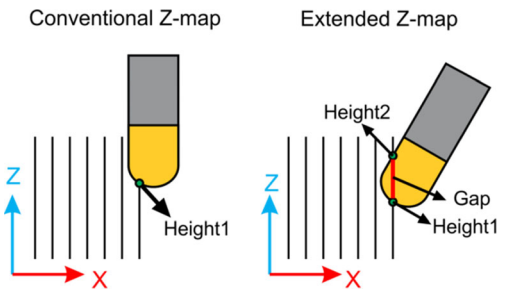

Fig. 12 Workpiece representations for Z-map approaches

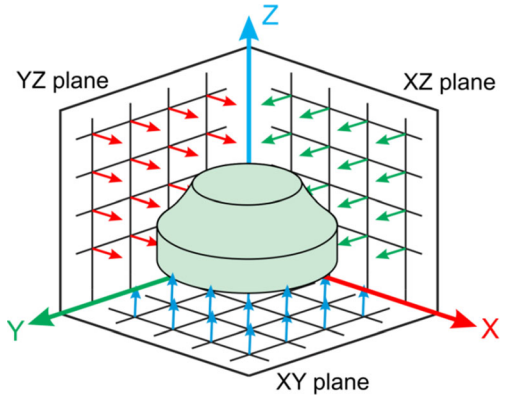

Fig. 13 Workpiece representation for three-orthogonal dexelfield approach

similar to extended Z-map approach. However, the depth buffer is applied in three orthogonal directions. In other words, three-orthogonal dexelfield approach utilizes Z-map, Y-map, and X-map simultaneously which is illustrated in Fig. 13.

The use of three-orthogonal dexelfield is quite critical since in extended Z-map approach, engagement region may not be obtained accurately due to the perpendicular intersection regions of the tool with the Z direction vectors. Therefore, in these regions, contact patch is truncated from the actual contact patch even if the verification resolution is high.

5 Implementation and results

Proposed cutter-workpiece extraction methods are implemented and tested for different types of toolpaths, blank workpieces, tools, and machining strategies in order to exploit the capabilities and demonstrate weak and strong points of engagement models.

The first toolpath is a 2.5-axis pocketing operation performed with end mill tool. Pockets of the aerospace body part

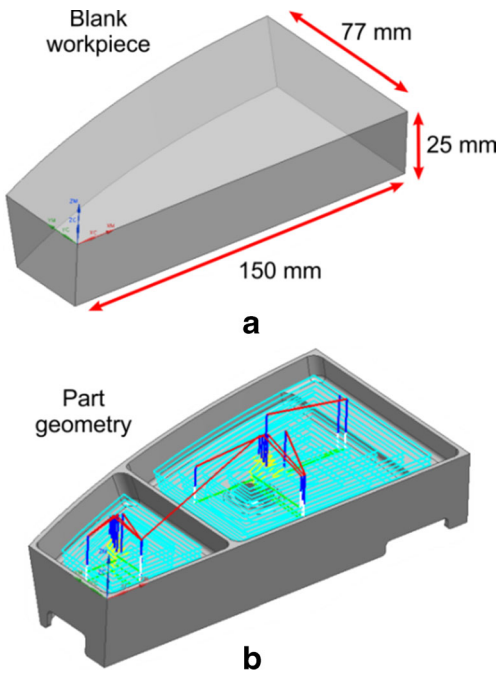

Fig. 14 Example 1: **a** blank workpiece and **b** part geometry and toolpath

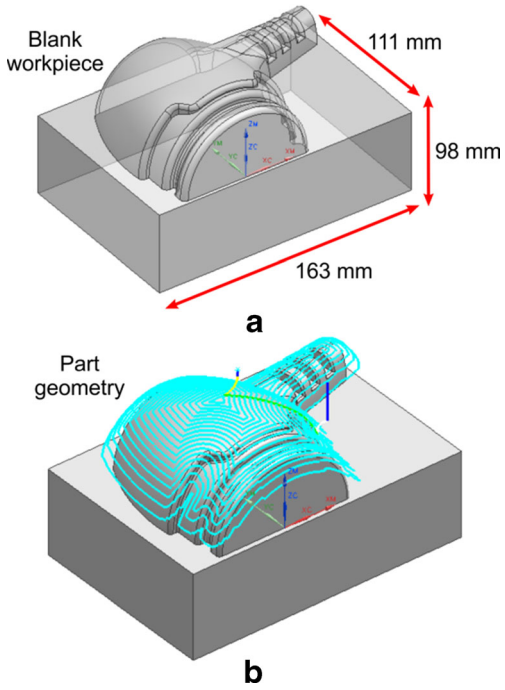

Fig. 15 Example 2: **a** blank workpiece and **b** part geometry and toolpath

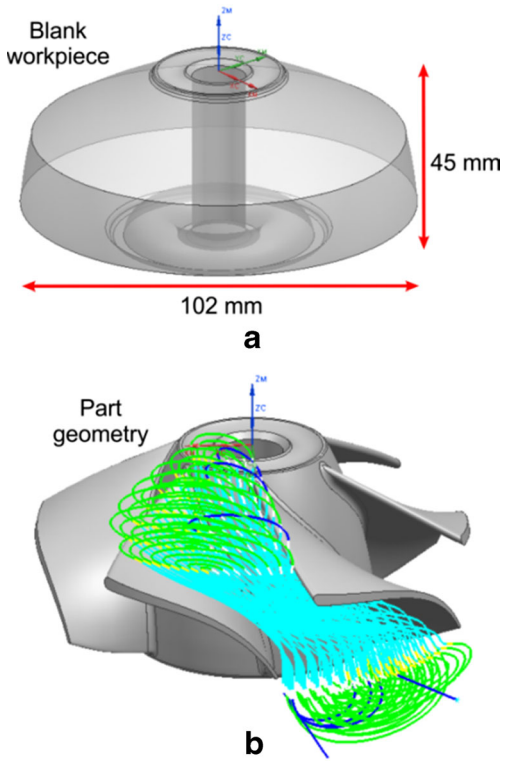

Fig. 16 Example 3: **a** blank workpiece and **b** part geometry and toolpath

Table 1 Resolution parameter for corresponding disk thicknesses

Disk thickness (mm)	0.05	0.1	0.133	0.15	0.2
Resolution (mm)	0.04	0.75	0.1	0.1	0.15

shown in Fig. 14 are machined with a 12-mm diameter end mill where global depth of cut is set to 2 mm resulting in 527 NC segments. Blank workpiece of the part is selected to be a nonrectangular block with the specified dimensions (Fig. 14). The second example presents a three-axis ball-end milling of a free-form surface. A non-steep surface contouring operation of the semi-finishing of a hair dryer mold is simulated. In this scenario, it is assumed that the stock workpiece for the part is produced by casting; therefore, blank workpiece is an offset part of the final geometry (Fig. 15). Stock material amount on the part is 1 mm. Cutting tool used in this example is a 16-mm ball-end mill. The number of cutter locations for this toolpath is 4209.

Final toolpath is a simultaneous five-axis ball-end milling toolpath for blisk geometry. During this operation, rough cutting of the hub of the blisk geometry is performed with an 8-mm diameter ball-end mill. Usually, stock workpieces for impellers and blisks are prepared by turning operation. Hence, blank workpiece for this example is geometry with an arbitrary shape which can be obtained by turning process (Fig. 16). During the operation, the distance between each cut level is constant and set to 3.5 mm; consequently, the depth of cut changes approximately between 0 and 4 mm. Specified toolpath consists of 6251 cutter locations (CL).

For practical applications, a geometric verification system has to provide fast, robust, and accurate calculation. The efficiency of a cutter-workpiece engagement system can be judged based on the computational performance and the accuracy of the method.

5.1 Comparison of performance

Each toolpath given in the previous section is simulated for different disk thickness values. Disk thickness value determines the order of the discretization of the contact patch obtained from the in-process workpiece. In three-orthogonal dexelfield approach, disk thickness is not a direct measure of the resolution parameter for simulations because disk thickness value and the resolution are independent of each other. As it is explained in Section 3, resolution for this method is specified as the distance between two consecutive dexel blocks (depth elements). Solid modeler-based engagement

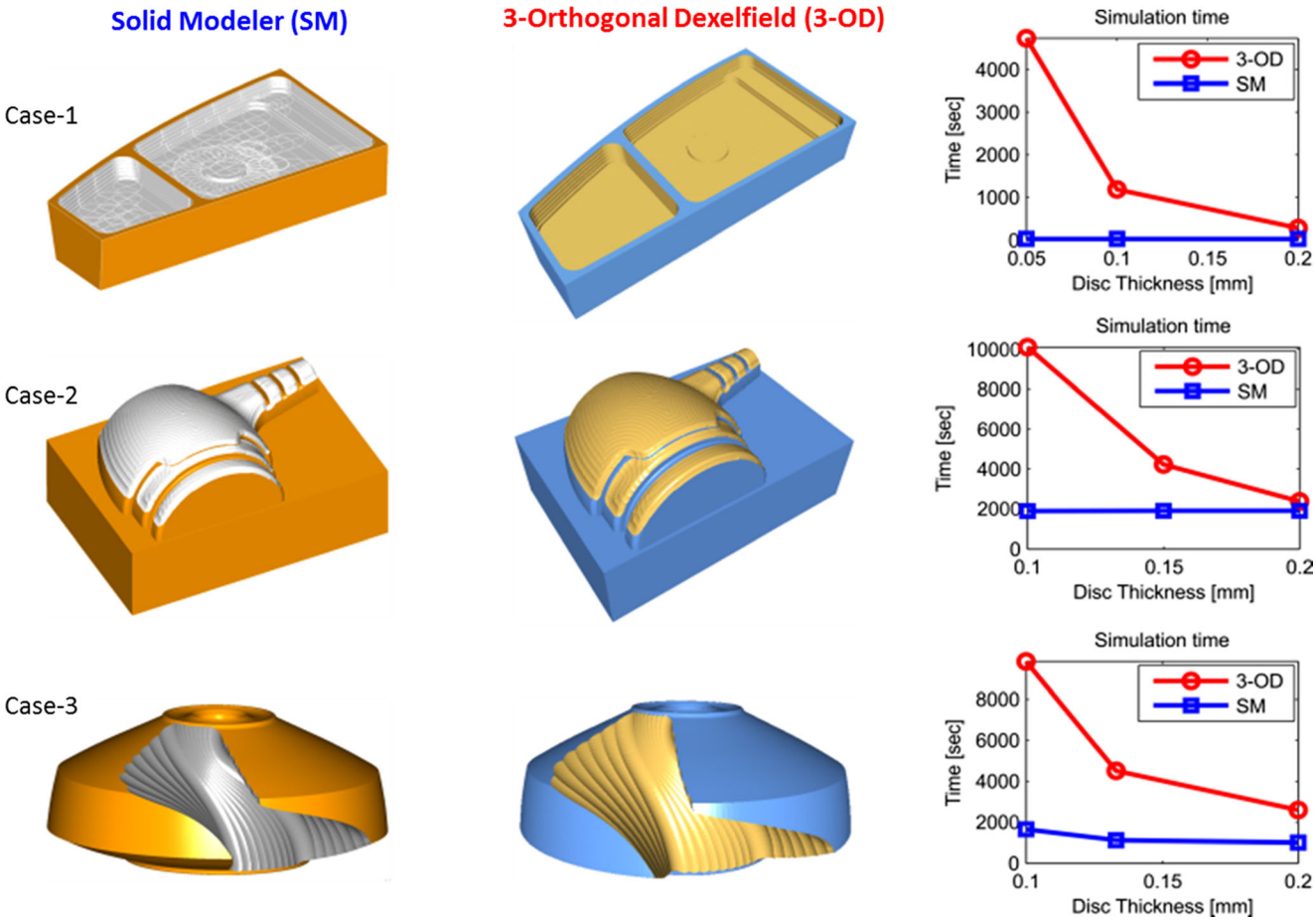

Fig. 17 Verification results and comparison of computation times

calculation scheme employs an exact representation of the tool swept envelope and its intersection between the in-process workpiece. Hence, resolution parameter is not applicable to solid modeler-based engagement method. For a fair comparison, disk thickness is utilized as determinant variable. After the determination of the disk thickness, appropriate resolution parameter for three-orthogonal dexelfield approach is set. Resolutions for the simulated toolpaths are shown in Table 1 with corresponding disk thicknesses.

Aforementioned toolpaths are simulated, and cutter-workpiece engagement maps are extracted from the cut geometry for three examples. Output machined surfaces and the graphical comparison of the computation times are given in Fig. 17 for two approaches. Verification results for three-orthogonal dexelfield approach are shown in Fig. 17. The simulations were performed with the lowest disk thickness (the highest resolution).

Results of all simulations are given in Table 2. According to the presented computation times, it is observed that for all simulation, computational efficiency of the solid modeler-based approach is superior to three-orthogonal dexelfield approach. For the 2.5-axis end milling operation (example 1), computation time of solid modeler-based approach is 8.6, 40.1, and 159.5 times faster for 0.05-, 0.1-, and 0.2-mm disk thicknesses, respectively. In three-axis ball-end milling toolpath (example 2), computation time of solid modeler-based approach is 0.25, 1.2, and 4.25 times faster for 0.1-, 0.15-, and 0.2-mm disk thicknesses, respectively. Similarly, five-axis machining simulations indicate that the computation time for solid modeler-based engagement scheme is up to 4.96 faster than three-orthogonal dexelfield scheme at the highest resolution.

5.2 Comparison of accuracy

The second important criterion, while judging the efficiency of the cutter-workpiece engagement model, is the accuracy of the model since precise determination of the engagement region is crucial for the calculation of material removal volume and the cutting forces. Cutting force is a function of tool-workpiece contact area where larger contact area results in higher cutting forces.

Engagement maps for the simulated toolpaths are presented in Figs. 18, 19, and 20 for randomly sampled cutter locations along the toolpaths. Accuracy comparisons are performed by comparing the outputs of the simulations with the highest resolutions. In Fig. 18, results of the 2.5-axis end milling of the aerospace body part are illustrated. In most of the CL points, three-orthogonal dexelfield approach calculated the engagement region less accurately resulting in a smaller engagement boundary. Three-axis ball-end milling of the hair dryer mold offered more promising results compared to 2.5-axis milling example. The boundaries of the obtained contact patches are almost identical, yet there are small differences.

Tool orientation in five-axis machining is not constant; therefore, more complex and dynamically changing contact with the workpiece may occur. For this reason, capability of an engagement approach may be better put to the test in five-axis machining. From the results shown in Fig. 20, it is obviously observed that the difference between the solid modeler and the three-orthogonal dexelfield approaches increased significantly. Especially in multiple engagement regions where the axial depth of cut is high, as seen in Fig. 20b, there is a substantial amount of misinterpretation of the contact region.

Table 2 Computation times for the toolpath examples

Case-1	dt (mm)	0.05	0.1	0.133	0.15	0.2
SM	Time (sec)	29.5	28.9	–	–	28.8
3-OD		4737	1188	–	–	278
Case-2	dt (mm)	0.05	0.1	0.133	0.15	0.2
SM	Time (sec)	–	1924	–	1911	1899
3-OD		–	10,115	–	4225	2381
Case-3	dt (mm)	0.05	0.1	0.133	0.15	0.2
SM	Time (sec)	–	1650	1113	–	1000
3-OD		–	9849	4501	–	2591

SM solid modeler-based method, *3-OD* 3-orthogonal dexelfield method, *dt* disk thickness

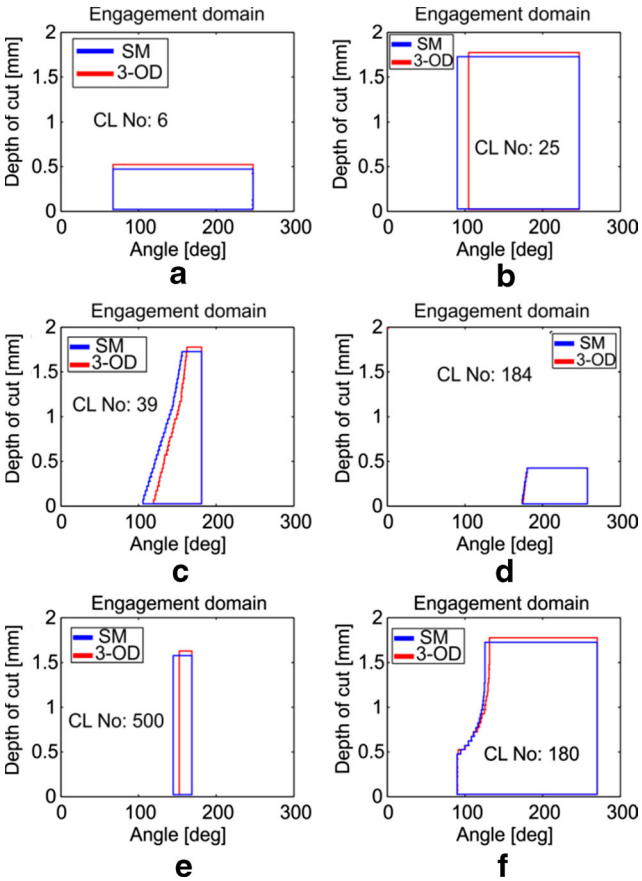

Fig. 18 **a**–**f** Accuracy comparison in 2.5-axis end milling for different CL points

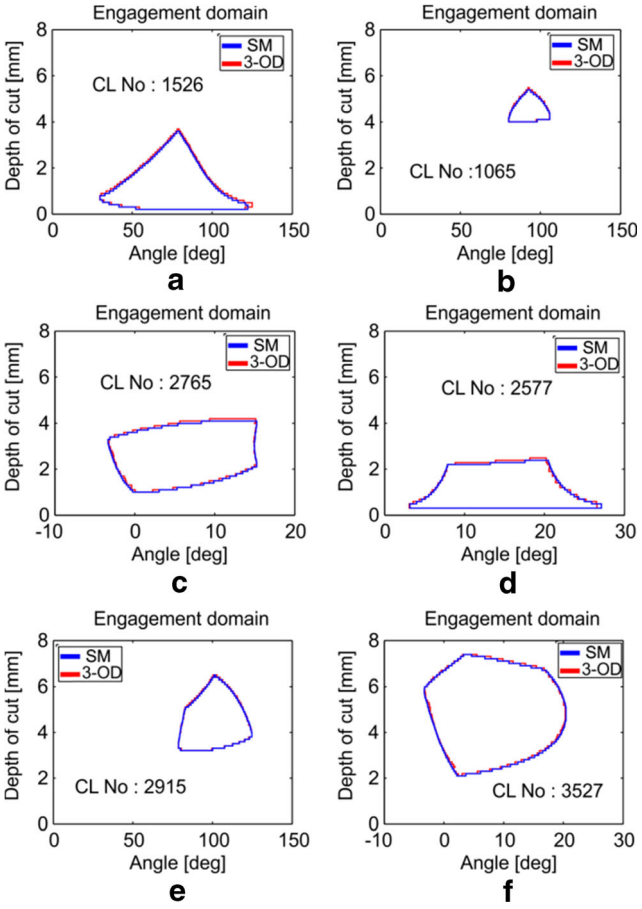

Fig. 19 **a**–**f** Accuracy comparison in three-axis ball-end milling for different CL points

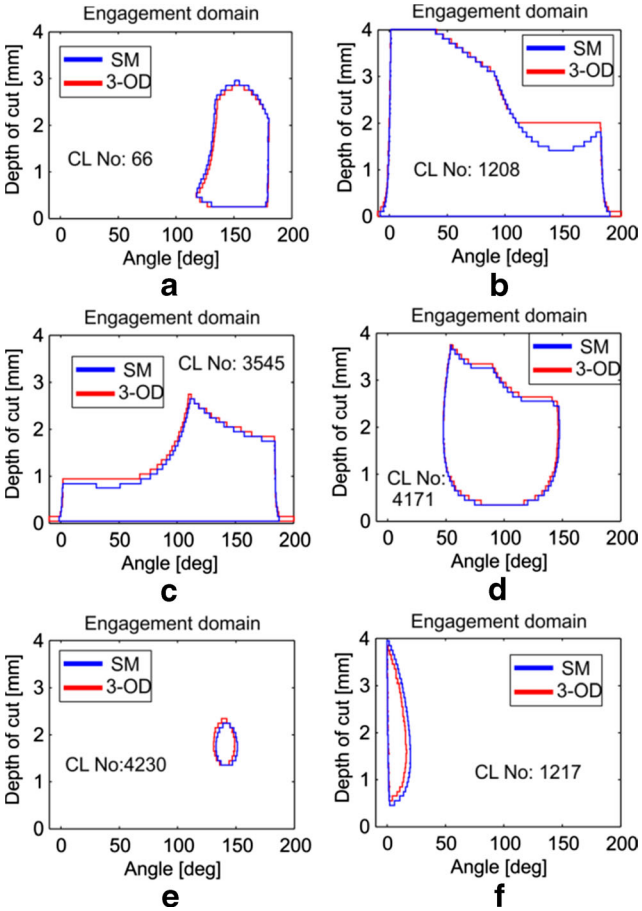

Fig. 20 **a**–**f** Accuracy comparison in five-axis machining for different CL points

In conclusion, solid modeler-based engagement model is superior to the three-orthogonal dexelfield approach. As it is illustrated in Figs. 18, 19, and 20, there are differences between the two methods, and it is observed that solid modeler-based approach is more accurate than the three-orthogonal dexelfield approach. Solid modeler-based approach uses exact Boolean operations between the cutter swept envelope and the workpiece; for this reason, surface patch boundaries are exact and smooth. In three-orthogonal dexelfield approach due to numerical instability and the nature of the intersections, fluctuations in the engagement angles and the trimming of the engagement region occur.

5.3 Example with simulated forces

In this section, an example application of the proposed engagement models is presented. Cutter-workpiece engagement maps are utilized as geometric information for cutting force prediction in NC machining. A five-axis simultaneous impeller hub roughing operation is first stimulated by engagement models, and the resulting engagement information is used for force prediction. Simulated toolpath consists of 1572 CL points with approximately 40 tool passes (Fig. 21)

Practical applications of the engagement models are performed via three- and five-axis cutting force models given in [18–21]. The results of the cutting force simulation are compared with experimental machining test data. Cutting forces are collected with a rotary dynamometer while the workpiece is being cut on a five-axis machine tool. Figure 22 shows the

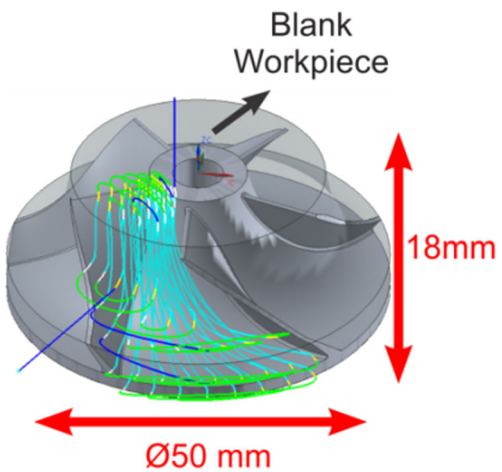

Fig. 21 Impeller hub roughing toolpath

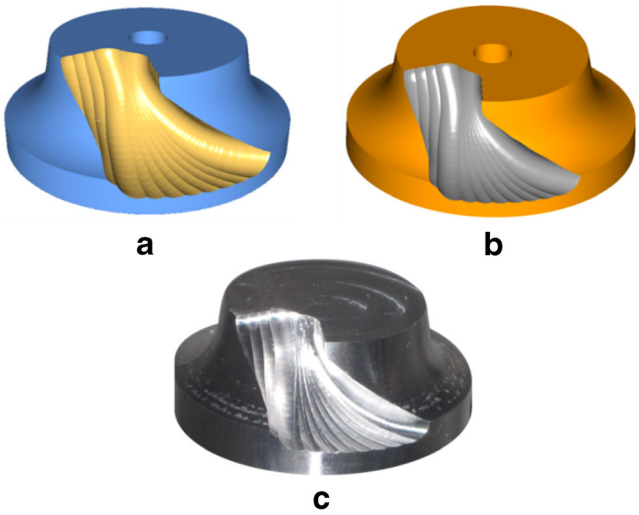

Fig. 22 Virtually machined workpiece: **a** three-orthogonal dexelfield, **b** solid modeler based, and **c** actual machined workpiece

virtual machining simulation results and the actual machined workpiece.

Simulations for both methods are performed for 0.1-mm disk thickness along the tool axis of the cutter. The computation time for the solid modeler-based engagement calculation is 213 s on a Windows Core2Duo, 1.8 GHz/4 GB personal laptop, whereas three-orthogonal dexelfield approach takes 56 min and 25 s on a Windows 7 64-bit, Core2Duo 3.16 GHz/8 GB desktop PC.

Comparison of the cutting force simulations with the experimental data is shown in Fig. 23. From the figure, it is observed that the solid modeler-based cutter-workpiece engagement methodology calculates the engagement domain more accurately. Force simulation results performed with the solid modeler-based engagement approach shows better agreement than three-orthogonal dexelfield approach not only in its trend but also in prediction accuracy.

The discrepancy in the cutting force simulations in three-orthogonal dexelfield approach is due to misinterpretation of

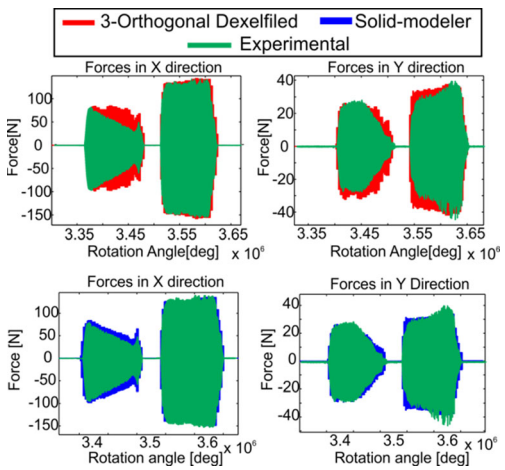

Fig. 23 Comparison of cutting force simulations

the multiple engagement regions. This method allows only in-quadrant multiple engagement region identifications. At low axial immersion regions, due to low simulation resolution, calculation accuracy may also be degraded.

6 Conclusion

Cutting forces in machining are determined by extracting the cutter-workpiece engagement (CWE) from the in-process workpiece in the form of start and exit angles as a function of axial height along the tool axis. Cutter-workpiece intersection determines the region where the tool actually removes material and creates cutting forces and vibrations. The geometry of an engagement domain plays a fundamental role in process modeling, and its shape and topology change due to complex workpiece, tool, and motion.

The current techniques for CWE calculation are fairly specialized and are applicable to restricted classes of motions such as 2.5- and three-axis motions, while practical and important complex five-axis milling cases do not have efficient and feasible solution methods. In this paper, both solid modeler-based and discrete CWE calculation methods for obtaining three- and five-axis milling with flat and ball-end mill tools are developed and presented. A novel discrete method, called three-orthogonal dexelfield, of obtaining CWE maps is developed. Three-orthogonal dexelfield uses the depth buffer in three orthogonal directions. In other words, three-orthogonal dexelfield approach utilizes Z-map, Y-map, and X-map simultaneously for improved accuracy. The second new method of calculating CWE maps uses B-rep modeler, Parasolid to perform Boolean operations, update the in-process workpiece, and calculate the intersection between cutter and workpiece.

In five-axis ball-end milling, due to variable tool axis orientation, complex workpiece, and tool geometry, the engagement region between the tool and the workpiece is very complex and irregular. Hence, developed solid modeler-based CWE model provides an efficient and accurate solution by utilizing the exact Boolean approach while extracting the engagement information from the in-process workpiece. Further increase in computation speed is obtained by this method.

References

1. Altintas Y, Kersting P, Biermann D, Budak E, Denkana B, Lazoglu I (2014) Virtual process systems for part machining operations. CIRP Ann 63(2):585–605
2. Chappel IT (1983) The use of vectors to simulate material removed by numerically controlled milling. Comput Aided Des 15:156–158
3. Hook TV (1986) Real-time shaded NC milling display. SIGG RAPH Comput Graph 20:15–20

4. Drysdale R, Jerard R, Schaudt B, Hauck K (1989) Discrete simulation of NC machining. Algorithmica 4:33–60
5. Jerard RB, Drysdale RL III, Hauck KE, Schaudt B, Magewick J (1989) Methods for detecting errors in numerically controlled machining of sculptured surfaces. IEEE Comput Graph Appl 9:26–39
6. Fussell BK, Jerard RB, Hemmett JG (2001) Robust feedrate selection for 3-Axis NC machining using discrete models. J Manuf Sci Eng 123:214–224
7. Fussell BK, Jerard RB, Hemmett JG (2003) Modeling of cutting geometry and forces for 5-axis sculptured surface machining. Comput Aided Des 35:333–346
8. Roth D, Gray P, Ismail F, Bedi S (2007) Mechanistic modelling of 5-axis milling using an adaptive and local depth buffer. Comput Aided Des 39:302–312
9. Voelcker HB, Hunt WA (1981) Role of solid modelling in machining-process modelling and NC verification SAE preprints
10. Spence AD, Altintas Y (1994) A solid modeller based milling process simulation and planning system. J Eng Ind 116:61–69
11. Spence AD, Abrari F, Elbestawi MA (1999) Integrated solid modeler based solutions for machining. In: Proceedings of the fifth ACM symposium on solid modeling and applications. ACM, Ann Arbor, pp 296–305
12. Imani BM, Sadeghi MH, Elbestawi MA (1998) An improved process simulation system for ball-end milling of sculptured surfaces. Int J Mach Tools Manuf 38:1089–1107
13. Imani BM, Elbestawi MA (2001) Geometric simulation of ball-end milling operations. J Manuf Sci Eng 123:177–184
14. Ferry W, Yip-Hoi D (2008) Cutter-workpiece engagement calculations by parallel slicing for five-axis flank milling of jet engine impellers. J Manuf Sci Eng 130:051011–051012
15. Du S, Surmann T, Webber O, Weinert K (2005) Formulating swept profiles for five-axis tool motions. Int J Mach Tools Manuf 45:849–861
16. Wang WP, Wang KK (1986) Geometric modeling for swept volume of moving solids. IEEE Comput Graph Appl 6:8–17
17. Kim GM, Cho PJ, Chu CN (2000) Cutting force prediction of sculptured surface ball-end milling using Z-map. Int J Mach Tools Manuf 40:277–291
18. Lazoglu I, Boz Y, Erdim H (2011) Five-axis milling mechanics for complex free form surfaces. CIRP Ann Manuf Technol 60:117–120
19. Erkorkmaz K, Layegh E, Lazoglu I, Erdim H (2013) Feedrate optimization for freeform milling considering constraints from the feed drive system and process mechanics. CIRP Ann 62:395–398
20. Manav C, Bank HS, Lazoglu I (2013) Intelligent toolpath selection via multi-criteria optimization in complex sculptured surface milling. J Intell Manuf 24:349–355
21. Lazoglu I, Layegh SE, Mamedov K A, Erdim H (2014) Process optimization via feedrate scheduling in milling. In: Laperrière L, Reinhart G (eds) CIRP encyclopedia of production engineering. Springer, pp 979–987